How Insoluble Inclusions and Intersecting Layers Affect the Leaching Process within Potash Seams

Svenja Steding[1,2], Thomas Kempka[1,2], and Michael Kühn[1,2]

[1]GFZ German Research Centre for Geosciences, Potsdam, Germany.

[2]University of Potsdam, Institute of Geosciences, Potsdam, Germany.

Corresponding author: Svenja Steding (ssteding@gfz-potsdam.de)

Key Points:

- Insoluble inclusions and interlayers in potash seams slow down the leaching zone growth in case of transport-dominated systems.
- Distribution of inclusions is of minor importance, while inclinations of intersecting layers are more relevant for risk assessment.
- Saturation-dependent dissolution rates change the leaching zone shape and should be considered for further scenario analyses.

Abstract

Potash seams are a valuable resource containing several economically interesting, but also highly soluble minerals. One of the major safety risks for subsurface mining operations is the formation of leaching zones which is controlled by the mineralogical composition and the dissolution rate of the salt rock. In the present study, a reactive transport model including mineral-specific, saturation-dependent dissolution rates is used to examine the influence of insoluble inclusions and intersecting layers. For that purpose, a scenario-analysis is carried out considering different rock distributions within a carnallite-bearing potash seam. The results show that the validity of the dimensionless Damköhler number (Da) decreases if insoluble areas become broader and more inclined. However, with regard to the growth rate of the leaching zone, the exact distribution of insoluble inclusions is of minor importance. While reaction-dominated systems (Da < 1) are not affected by these at all, the dissolution front of transport-dominated systems (Da > 1) advances more slowly compared to homogeneous potash seams. However, the ratio of permeated rock in vertical direction becomes higher. Accordingly, heterogeneous potash seams are beneficial with regard to risk assessment as long as the mechanical stability of the leaching zone is given. For determining dissolution rates, saturation-dependency should always be considered as it increases the hazard potential in the long-term. Literature data confirm the simulation results and indicate that most systems in nature are transport-dominated. To investigate the effects of mineral heterogeneity in further detail, more experimental data on the dissolution kinetics of potash salt are required.

1 Introduction

The role of potash seams within salt deposits can be viewed from different perspectives: on the one hand, they are a valuable resource that has been mined for many decades, while on the other hand, they represent a potential risk for technical caverns and subsurface waste repositories (Warren, 2017). However, both perspectives have in common that the formation of leaching zones within potash seams is considered as highly critical. Due to the increased solubility of potash salt, leaching zones can grow relatively fast and jeopardise the integrity and mechanical stability of mines or technical caverns (Prugger & Prugger, 1991; Boys, 1993; Keime et al., 2012; Mengel et al., 2012). In order to describe their temporal and spatial evolution, reactive transport models are required (Dijk & Berkowitz, 2000). Steding et al. (2021) showed that the Péclet (Pe) and Damköhler (Da) numbers represent useful indicators to evaluate growth rates, shapes and mineralogical compositions of leaching zones within potash seams, providing a basis to estimate the hazard potential. However, so far only homogeneous potash seams have been investigated. Studies for rock salt and other minerals indicate that local variations in the proportion of potash minerals as well as inclusions or layers of insoluble materials may have a significant influence on shapes and growth rates (Thoms & Gehle, 1999; Li et al., 2018; Jinlong et al., 2020; Liu et al., 2017; Wei et al., 2019).

This study focusses on how heterogeneities in the form of inclusions and intersecting layers of pure halite (further referred to as halitic areas) affect the evolution of leaching zones within potash seams. The reactive transport model presented by Steding et al. (2021) is used to perform a scenario analysis under density-driven flow conditions. Six different mineral distributions are investigated with halitic areas ranging from several small inclusions to one continuous layer. Inclined layers are examined as well, since these may cause an asymmetric expansion of leaching zones (Fokker, 1995). The penetrating solution is assumed to be NaCl-

saturated, i.e. halitic areas are basically insoluble, what makes them acting as impermeable barriers. This is expected to considerably change the hydrodynamic conditions and saturation distribution within leaching zones. To quantify these effects, the temporal and spatial leaching zone evolutions are analysed and compared to that of a homogeneous potash seam. Furthermore, the maximum dissolution rate of potash salt is varied by two orders of magnitude to identify the differences between reaction-dominated (Da < 1) and transport-dominated (Da > 1) systems. Additionally, the interchange approach (Steding et al., 2021) was extended to include saturation-dependent dissolution rates. The aim of our study is to find out how insoluble layers and inclusions influence the evolution and hazard potential of leaching zones, and if a classification based on the Pe and Da numbers is still possible in case of heterogeneous mineral distributions.

2 Materials and Methods

The concept of the applied reactive transport model is shown in Figure 1. Each simulation time step starts with the solution of the partial differential equations for fluid flow and transport of chemical species using the TRANSport Simulation Environment (TRANSE) (Kempka, 2020). TRANSE is coupled with the geochemical reaction module PHREEQC (Parkhurst & Appelo, 2013) applied in combination with the THEREDA database (Altmaier et al., 2011). In the second calculation step, PHREEQC is used to update fluid densities and mineral saturations after transport. After that, a step called „interchange“ is performed which describes the dissolution of minerals from (nearly) dry into permeated cells and allows the dissolution front to move forward (Steding et al., 2021). The terms „dry“ and „permeated“ are used in view of the fluid saturation in the pore space, while the term „saturated“ refers to the chemical equilibration of the solution with respect to salt minerals. In the final calculation step, the chemical reactions resulting from transport and interchange are determined using PHREEQC. Thereby, thermodynamic equilibrium is assumed within each cell. The updated concentrations and fluid properties, such as density and viscosity, are then transferred back to TRANSE to calculate flow and transport in the next simulation time step (Figure 1). More details on this procedure are presented in Steding et al. (2021). The interchange of minerals and solution has been extended in the present study and will be described in detail in the following subsection.

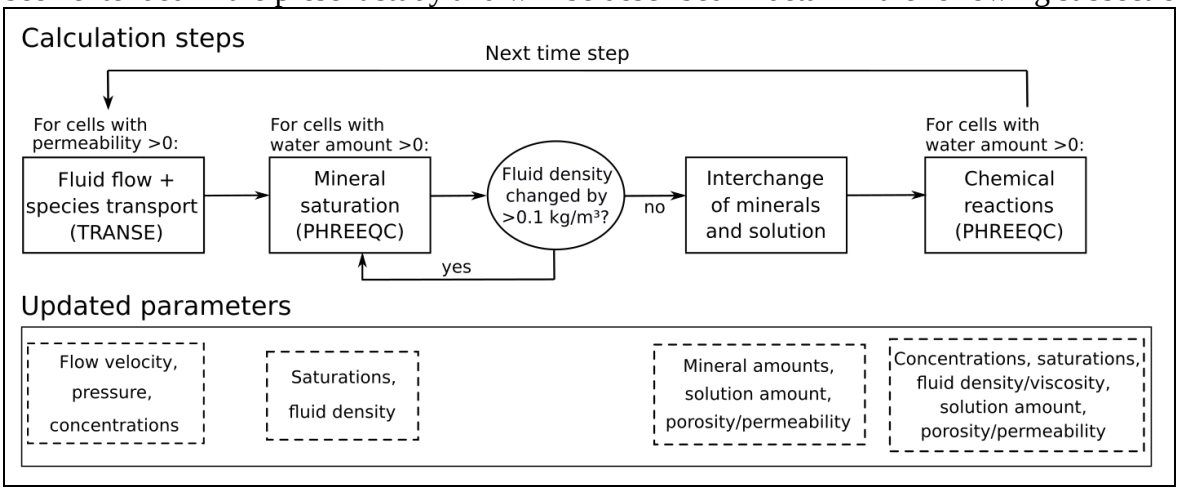

Figure 1. Flow sheet of the coupled reactive transport model: calculations undertaken at each simulation time step and associated output parameters (modified from Steding et al., 2021).

2.1 Extended interchange approach

In Steding et al. (2021), constant dissolution rates were used to calculate the interchange of salt minerals. However, it is known that close to equilibrium the dissolution rates decrease considerably (Durie & Jessen, 1964; Röhr, 1981; Palandri & Kharaka, 2004). Based on the results of Alkattan et al. (1997), a linear saturation-dependency is assumed:

$$rate = k_{max} \cdot (1 - \Omega) \qquad \text{with } \Omega = {}^{Q}/_{K} = 10^{SI} \qquad (1)$$

and k_{max} (cm/s) as dissolution rate in an infinitely dilute solution. Q is the activity product and K the equilibrium constant. The saturation index SI (-) results from log(Q/K). Since the maximum dissolution rate k_{max} as well as the saturation state vary across minerals, an average dissolution rate for the potash seam (Figure 2a) is not applicable here. Instead, the dissolution rate rate (cm/s) and the amount of minerals dissolved into an adjacent cell Min_{sol} (mol) need to be calculated individually for each mineral (Figure 2b). Thereby, rate always refers to the saturation state of the solution the mineral is dissolved into. Between Cell A and Cell B the amount of interchanged mineral *n* is calculated by equation (2):

$$Min_{sol,n} = rate_n \cdot Min_{A,n}/di \cdot (\Phi_B - \Phi_A)/(1 - \Phi_A) \cdot dt \qquad (2)$$

The amount of mineral *n* present in Cell A, $Min_{A,n}$ (mol), divided by the cell diameter perpendicular to the dissolution front *di* (cm) gives the affected amount of mineral *n* if the width of 1 cm is dissolved from Cell A. To take into account the contact area between the rock in Cell A and the solution in Cell B, this amount is multiplied with the porosity difference between both cells $(\Phi_B\text{-}\Phi_A)$ and divided by the volume fraction of the rock in Cell A $(1\text{-}\Phi_A)$. If $\Phi_A \geq \Phi_B$, the interchange is zero, i.e. minerals can only be dissolved into adjacent cells with higher porosity. *dt* (s) is the length of the simulation time step. If the solution in Cell B is already saturated with respect to *n*, raten becomes zero and the mineral is not dissolved. The interchange takes place at each interface between two cells within the model. The volumes of all minerals dissolved at one interface are cumulated to determine the amount of solution that is transferred in return to keep the volume of both cells constant (Figure 2).

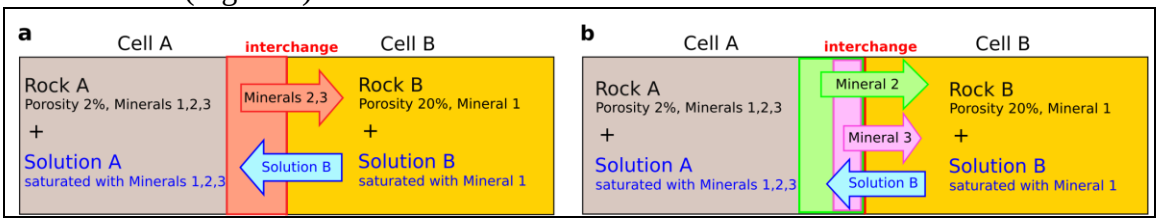

Figure 2. Sketch of the interchange approach with (a) constant and (b) variable dissolution rates. A defined amount of each mineral according to equation (2) is dissolved from a cell with low porosity (Cell A) into an adjacent cell with higher porosity (Cell B). These amounts are cumulated and the solution is transferred into the cell with lower porosity to fill the newly formed pore space (modified from Steding et al., 2021).

At the dissolution front, the interchange approach enables originally dry cells to receive solution for the first time from an adjacent cell (Figure 3a). The solution needs to be undersaturated with at least one of the minerals from the dry rock, otherwise no

interchange takes place. Newly permeated cells are divided into a permeated and a dry sub-cell to avoid an immediate drying out due to high solid-fluid-ratios (Figure 3b). In case of constant dissolution rates, all minerals in the permeated part were assumed to be in equilibrium with the solution of the cell, while minerals in the dry part are not considered in the subsequent calculation of chemical reactions (Steding et al., 2021). However, as shown in Figure 3a, the varying dissolution rates challenge the identification of a clear borderline between dry and permeated or equilibrated and non-equilibrated parts, respectively. In can be seen that Mineral 2 has the highest dissolution rate, and therefore limits the region of increased porosity where mineral solution occurs (green). Within this region, it is reasonable to equilibrate the solution with regard to Mineral 2. However, Mineral 3 has a lower dissolution rate, and can therefore only be equilibrated with the solution in the pink subregion. Following this reasoning, one would end up with an additional subregion for each mineral, which is of course not practical. Instead, the permeated part within each cell is split up into minerals that are in equilibrium with the solution (equilibrated minerals Min_{eq}) and such that are not (non-equilibrated minerals Min_{neq}) (Figure 3b). Thereby, the volume of the permeated part V_{per} is determined by the most soluble mineral (Mineral 2, green area). Outside of this area, the salt rock is still dry and the composition Min_{dry} corresponds to the originally unaffected potash seam. In contrast, minerals within the permeated area V_{per} are surrounded by solution, whereby it is not yet in equilibrium with all minerals. Minerals that remain undissolved during the interchange due to their lower dissolution rates (Mineral 1 and parts of Mineral 3 within the green area, Figure 3a) are assigned to the non-equilibrated minerals Min_{neq}. In contrast, precipitations from Solution B belong to the minerals equilibrated with the solution Min_{eq}.

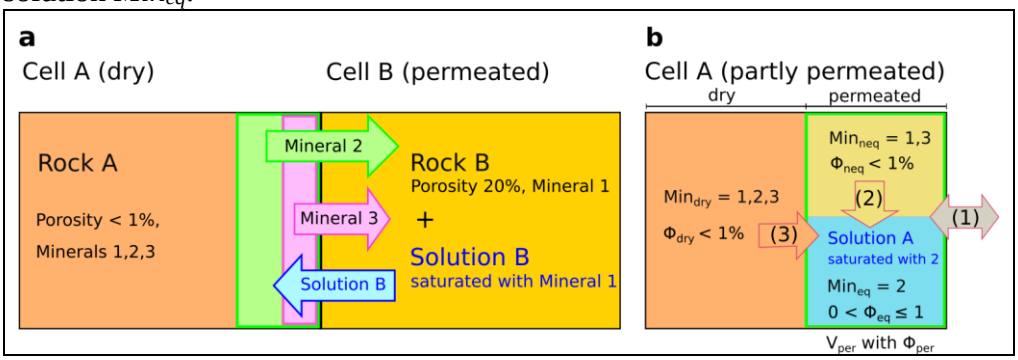

Figure 3. Sketch of the interchange at the dissolution front (a) resulting in a partly permeated cell (b). The permeated part V_{per} contains minerals Min_{eq} that are in equilibrium with Solution A and minerals Min_{neq} that are not. Besides interchange with adjacent cells (1), the internal dissolution of non-equilibrated minerals (2) and dry minerals (3) is considered following equations (2), (4) and (5) (modified from Steding et al., 2021).

In case of partly permeated cells, three different types of dissolution can occur (Figure 3b): the first one is the interchange with (fully permeated) adjacent cells according to Equation (2). For this, all three mineral compositions Min_{dry}, Min_{eq} and Min_{neq} are added up to determine Min_A. Φ_A is the average porosity of the cell calculated from the volume of Min_A related to the cell volume. If the partly permeated cell shows a higher average porosity than the fully permeated one, the interchange of minerals is

possible in reverse direction as well. The dissolved amount of each mineral is split among Min_{dry}, Min_{eq} and Min_{neq} according to their contribution to the total amount of this mineral. The solution transferred in return is mixed with the pre-existing solution in the permeated part. The chemical reactions resulting from the mixing and the following equilibration with Min_{eq} are determined after the interchange (Figure 1).

In addition to the interchange, internal dissolution processes within cells containing dry (Min_{dry}) or non-equilibrated (Min_{neq}) minerals need to be taken into account (Figure 3b). The interface area between a dry part and the adjacent permeated part(s) is assumed to be constant over time. At the beginning, when the cell is completely dry, the only adjacent permeated area is the neighbour cell and dry minerals can only be dissolved via interchange. Accordingly, the interface area is the interface between both cells, which is the cell width multiplied by its height. As V_{per} increases, Min_{dry} makes up a smaller part of the total mineral amount within the partly permeated cell and its interchange amount decreases. At the same time, the interface area between the dry and permeated parts within the partly permeated cell increases enhancing the internal dissolution of dry minerals. To account for that, the permeation state of the cell S_{per} (-) is calculated referring to the volume of the permeated part V_{per} in relation to the cell volume V_{cell}:

$$S_{per} = V_{per}/V_{cell} \tag{3}$$

The higher S_{per}, the more of the dry rock is dissolved into the solution of its own cell (by internal dissolution) instead of the adjacent cell (by interchange). Equation (4) is used to determine the amount of mineral *n* dissolved from Min_{dry} into the solution within the permeated part:

$$Min_{sol,dry,n} = rate_n \cdot Min_{dry,n}/\left(di \cdot \left(1 - S_{per}\right)\right) \cdot \Phi_{per} \cdot S_{per} \cdot \ dt \cdot \tag{4}$$

Generally, equation (4) is identical to equation (2), but multiplied by the permeation state S_{per}. *rate* is calculated from the saturation state within the partly permeated cell using equation (1). In order to determine the affected amount of mineral *n* if a width of 1 cm of the dry part is dissolved, the present amount, $Min_{dry,n}$ (mol), is divided by the diameter of the dry part perpendicular to the dissolution front. Therefore, the cell diameter *di* (cm) is now multiplied by the volume ratio of the dry part $(1-S_{per})$. The porosity within the dry part is nearly zero, simplifying the term $(\Phi_B - \Phi_A)/(1 - \Phi_A)$ in equation (2) to Φ_B, which equals the average porosity of the permeated part Φ_{per}. The dissolved amount of each mineral $Min_{sol,dry}$ is added to Min_{eq}. The same applies to precipitations resulting from the equilibration after the interchange (Figure 1). Similar to the interchange of dry minerals, the highest dissolution rate according to equation (1) determines the volume that is newly added to the permeated part V_{per} (Figure 3). For minerals with lower dissolution rates, the difference between the amount within this volume and the dissolved amount is added to Min_{neq}.

Finally, the internal dissolution of non-equilibrated minerals (Min_{neq}) has to be taken into account (Figure 3b). These minerals belong to the permeated part of a cell and are already surrounded by solution. However, when the area is permeated for the first time, their dissolution rate is too low to dissolve all minerals. Basically, there are two possible reasons for this: either the maximum dissolution rate k_{max} is (much) lower than

that of the other minerals, or the solution is already (nearly) saturated with these. In the latter case, one could add them to Min_{eq} without changing the solution or rock composition of the permeated part. However, the solution composition changes over time and originally saturated minerals may become undersaturated. In this case, an immediate equilibration could induce errors because the lower dissolution rates would be neglected. To account for the variation of dissolution rates, Min_{neq} is added stepwise to the solution. The dissolved amount $Min_{sol,neq}$ (mol) of each mineral is determined by equation (5):

$$\begin{aligned} Min_{sol,neq,n} &= rate_n \cdot Min_{neq,n}/V_{neq} \cdot contact\_area \cdot dt \\ &= rate_n \cdot Min_{neq,n}/V_{neq} \cdot factor \cdot di \cdot 1m \cdot \Phi_{eq} \cdot S_{per} \cdot dt \end{aligned} \quad (5)$$

The rate law is similar to those used for interchange (equation 2) and internal dissolution of dry minerals (equation 4). Again, *rate* (cm/s) is calculated from the saturation state within the partly permeated cell according to equation (1). Min_{neq} (mol) divided by the volume of the non-equilibrated minerals V_{neq} (cm³) and multiplied by the contact area between non-equilibrated minerals and solution (cm²), what gives the amount of mineral *n* if a width of 1 cm of the non-equilibrated minerals is dissolved. V_{neq} is calculated from the mineral amounts and densities in Min_{neq}, neglecting small porosities. However, the contact area between non-equilibrated minerals and solution is hard to determine, since the pore structure and spatial arrangement of the different minerals in the original rock are unknown. Therefore, a variable called *factor* (-) is introduced. If it is set to 1, a rectangular contact area similar to that between Min_{dry} and the solution (equation 4) is assumed. This can be seen as a minimum value. If precipitations do not block the access to Min_{neq}, the contact area to the solution flowing between the non-equilibrated minerals should be several times higher. Therefore, it can make sense to simplify the approach and to directly add Min_{neq} to Min_{eq}. In this case, it is assumed that the contact area is large enough to immediately equilibrate minerals and solution within an originally dry volume as soon as the first mineral has been dissolved from it. However, this is only realistic if the maximum mineral dissolution rates do not vary by several orders of magnitude. Furthermore, the first mineral dissolved should make up more than a few vol.% of the dry rock in order to create a sufficiently large contact area. If this is not the case, the internal dissolution of non-equilibrated minerals has to be considered. For some minerals, this may take much longer than the permeation of the cell, i.e. fully permeated cells can still contain non-equilibrated minerals (Figure 4). For the interchange according to equation (2), Min_{eq} and Min_{neq} are added up to

238 determine Min_A and Φ_A is defined as the average porosity of equilibrated and non-
239 equilibrated areas.

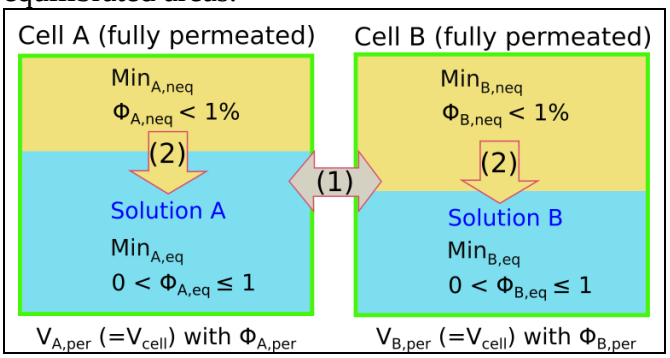

240 **Figure 4**. Fully permeated cells can still contain non-equilibrated minerals due to their
241 lower dissolution rates. Internal dissolution (2) within a cell reduces the amount of non-
242 equilibrated minerals; additionally they are considered for interchange (1). The average
243 porosity of the permeated part Φ_{per} corresponds to the average porosity of the cell and is
244 used for interchange as well as for flow and transport calculations.

245 Generally, it is assumed that minerals belonging to Min_{eq} are first dissolved if an
246 undersaturation occurs. As a result, the interchange or internal dissolution of minerals
247 present in Min_{eq} is not possible. Chemical reactions resulting from the processes
248 described above are determined in the final calculation step of the simulation (Figure 1).
249 Thereby, thermodynamic equilibrium is assumed in every cell. The average porosity of
250 the cell is always used in the flow and transport simulation step.

251 ## 2.2 Scenario analyses

252 In order to study the influence of heterogeneities, the leaching process of a
253 carnallite-bearing potash seam containing halite layers or inclusions is simulated.
254 Carnallitite is a very common, globally occurring potash salt with carnallite ratios of up
255 to >80 wt.%. Its leaching behaviour for homogeneous rock compositions has been
256 studied by Steding et al. (2021), and it was found that the evolution of the leaching zone
257 can be described based on the Péclet (Pe) and Damköhler (Da) numbers. Most common
258 and also most critical in the short term with regard to hazard potential are transport- and
259 advection-dominated systems (Da > 1 and Pe > 2), resulting from porosities ≥10% and
260 dissolution rates $\geq 10^{-5}$ cm/s. However, reaction- and advection-dominated systems (Da <
261 1 and Pe > 2) can be more critical in the long term, since flow barrier formation does not
262 occur. Both cases are investigated in this study to identify possible differences in the
263 effect of heterogeneities.

264 In all scenarios, the carnallite-bearing potash seam consists of 25 wt.% carnallite,
265 72 wt.% halite and 3 wt.% sylvite, corresponding to the volume fractions shown in Figure
266 5. If it gets into contact with NaCl brine, carnallite is always dissolved first causing a

precipitation of sylvite and halite (Koch & Vogel, 1980). Equation (6) gives the overall reaction:

$$KMgCl_3 \cdot 6H_2O + brine\ (NaCl) \rightarrow KCl + NaCl\ (brine) + brine\ (MgCl_2, KCl, NaCl) \quad (6)$$

According to Steding et al. (2021), 25 wt.% carnallite are sufficiently high to produce Péclet numbers >2 and low enough to ensure that Darcy flow is maintained while the mechanical stability of the porous leaching zone is not compromised. The densities and dissolution properties of the minerals are provided in Table 1. The dissolution rate k_{max} strongly depends on the hydrodynamic boundary conditions: it increases with flow velocity (Yang et al., 2017), and reaches values under turbulent flow conditions that are at least one order of magnitude higher than for laminar flow (Durie & Jessen, 1964; Alkattan et al., 1997). This is due to most salt minerals showing transport-controlled dissolution behaviour, i.e. k_{max} is controlled by the thickness of the diffusive boundary layer at the mineral surface (Hoppe & Winkler, 1974; Alkattan et al., 1997; De Baere et al., 2016). The boundary layer thickness, and consequently k_{max}, depend on the flow velocity, diffusion coefficients and surface roughness (Dreybrodt & Buhmann, 1991; Raines & Dewers, 1997; Ahoulou et al., 2020; Dutka et al., 2020). Based on the values of Röhr (1981), an average k_{max} of $5 \cdot 10^{-4}$ cm/s is applied to all three minerals in Table 1. However, this is an upper value since it refers to convection in open cavities. It can be expected that convection within a porous leaching zone results in smaller flow velocities, and therefore in smaller dissolution rates. Accordingly, a second k_{max} of $5 \cdot 10^{-6}$ cm/s is taken into account to ensure that both, transport- (Da > 1) and reaction-dominated (Da < 1) systems are investigated (Steding et al., 2021).

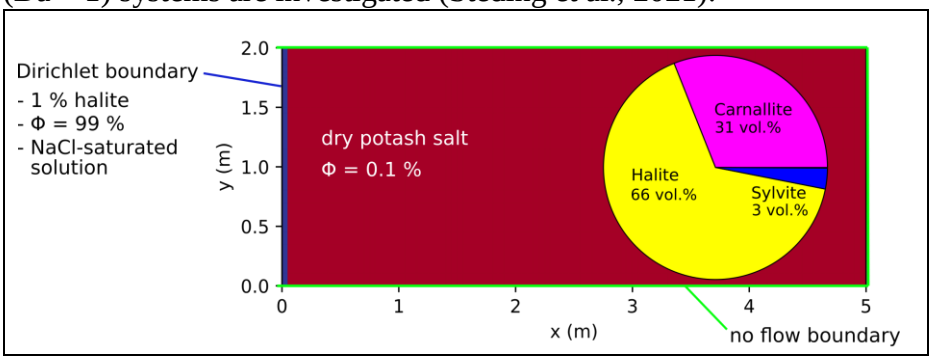

Figure 5. Initial and boundary conditions: the inflow region is prescribed by a Dirichlet boundary (blue line); all other boundaries are impermeable (green lines); the models are

initialised as dry with homogeneous potash salt (red, mineralogical composition shown) and halite inclusions according to Figure 6 (modified from Steding et al., 2021).

Table 1. Potash salt mineral densities and dissolution properties (modified from Steding et al., 2021).

Mineral	Density (kg/m^3)	Reaction equation (dissolution)	Log K
Carnallite	1600	$KMgCl_3 \cdot 6H_2O \rightarrow 3Cl^- + 6\ H_2O + K^+ + Mg^{2+}$	4.33
Halite	2170	$NaCl \rightarrow Cl^- + Na^+$	1.586
Sylvite	1990	$KCl \rightarrow Cl^- + K^+$	0.915

The 2D model height is 2 m, representing the typical thickness of potash seams in Germany, while the model width is 5 m with a discretization of 101 x 41 cells (Figure 5). At the start of the simulation, the entire model consists of dry potash salt with a porosity of 0.1%. Natural caverns and leaching zones are commonly formed in the vicinity of tectonic fault systems which enable fluid migration (Höntzsch & Zeibig, 2014). Due to the fact that the ascending solution has to cross several rock salt layers before it reaches the potash seam, it is usually NaCl-saturated. To represent such a fault zone, a Dirichlet boundary condition is used (Figure 5). It maintains a constant solution composition and porosity at the left model boundary, assuming a high fluid and mineral exchange rate within the fault zone. The other boundaries are considered as impermeable without any pre-defined pressure gradient applied. The 2D model makes use of the horizontally symmetric expansion of leaching zones to be expected if a potash seam has the same composition in both horizontal directions. Seen from the fault zone, the starting point of the leaching process, only one direction is simulated by taking advantage of the symmetry to reduce the required computational time.

Generally, the local variation of mineral proportions within carnallite-bearing potash seams is relatively low. However, heterogeneities in the form of inclusions or intersecting layers of (nearly) pure halite are a regular occurrence. Due to the fact that the solution leaving the fault zone is already NaCl-saturated, halite is usually not dissolved from the potash seam (Koch & Vogel, 1980; Steding et al., 2021). Accordingly, areas of pure halite act as barriers and affect the flow field of the leaching zone. To investigate their influence on the leaching zone evolution and its hazard potential, six different distributions are considered. As shown in Figure 6, the first three represent a potash seam (red) with intersecting layers of halite (grey). These layers are 30 cm thick and show inclinations of 0° or ±10°, respectively (Figures 6a-c). To ensure that boundary conditions are comparable, the layers always start at the same height at the centre of the fault zone. In the other three cases, the potash seam contains halite inclusions ranging from 10 cm x 10 cm (Figure 6d) to nearly continuous, horizontal layers (Figure 6f). Their distribution is created with GSTools (Müller & Schüler, 2021) using correlation lengths of 2:1, 17:0.5 and 34:1 in horizontal direction. In all six cases, the halitic area makes up between 13% and 15% of the potash seam and the surrounding potash salt is

homogeneous with the composition shown in Figure 5. For comparison, an additional case without any halitic areas is considered.

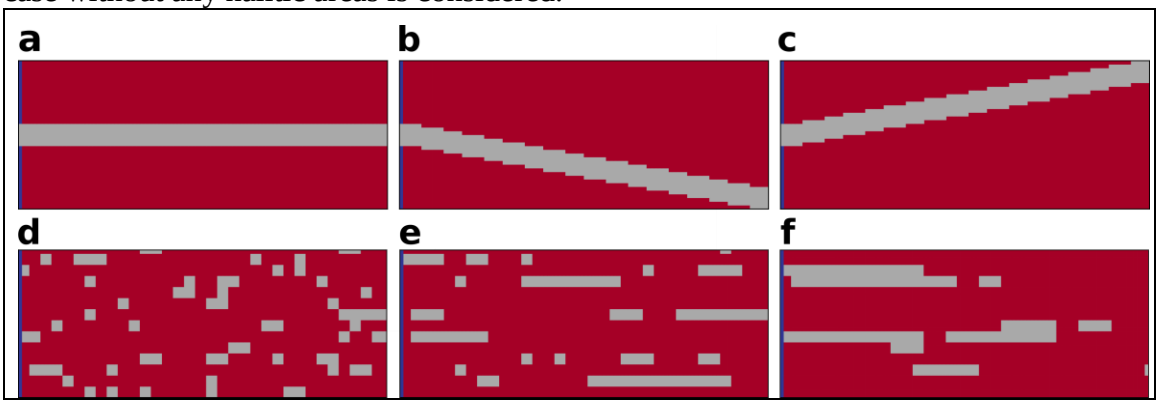

Figure 6. Heterogeneous rock distributions examined: The homogeneous potash salt (red) shown in Figure 5 is veined by layers with (a) 0°, (b) +10°, (c) -10° inclination or inclusions of pure halite with correlation lengths of (d) 2:1, (e) 17:0.5 and (f) 34:1 that make up 13-15% of the potash seam.

Following equation (6) and the volume ratios presented in Figure 5, maximum final porosities of around 30% can be expected (Steding et al., 2021). The porosity-permeability relationship by Xie et al. (2011) is used with a maximum permeability of $2 \cdot 10^{-11}$ m^2 (≈30% porosity) being applied. Since carnallite is dissolved first and making up >30% of the rock volume, a relatively large contact area between the solution and remaining minerals, sylvite and halite, can be assumed. Both minerals show the same maximum dissolution rate k_{max} as carnallite, facilitating a quick equilibration in case of under-saturations. Therefore, non-equilibrated minerals are neglected in this study. Instead, sylvite and halite are immediately added to the equilibrated part Min_{eq} as soon as the carnallite in their surroundings is dissolved. The diffusion coefficients of all four transported species Na^+, Cl^-, K^+ and Mg^{2+} are assumed to be equal and constant: an average value of $D_f = 1.5 \cdot 10^{-9}$ m^2/s is chosen based on Yuan-Hui and Gregory (1974). The fluid compressibility is set to $c_f = 4.6 \cdot 10^{-10}$ 1/Pa. Since temperature differences are negligible for a model height of 2 m, all simulations are undertaken at isothermal conditions at a temperature of 25 °C. Accordingly, the density-driven convective flow exclusively occurs due to dissolution and precipitation processes. The formation of leaching zones is simulated until the right model boundary is reached by the reaction front.

3 Results

Figure 7 shows the evolution of the ratio between permeated and total rock volume (halitic areas not included). In case of low dissolution rates ($k_{max} = 5 \cdot 10^{-6}$ cm/s), the leaching zone growth is nearly linear (Figure 7a,b). For all rock distributions, it takes 13-14 years for the simulations to meet the stop criterion with 96% of the (non-halitic) rock being permeated. Only in case of the +10° inclination, the growth rate starts to decrease after approximately six years (Figure 7a) with only 85% of the rock being permeated at the end. Halite inclusions lead to a less

regular growth rate compared to the homogeneous case, but strong deviations from linear growth are not observed (Figure 7b).

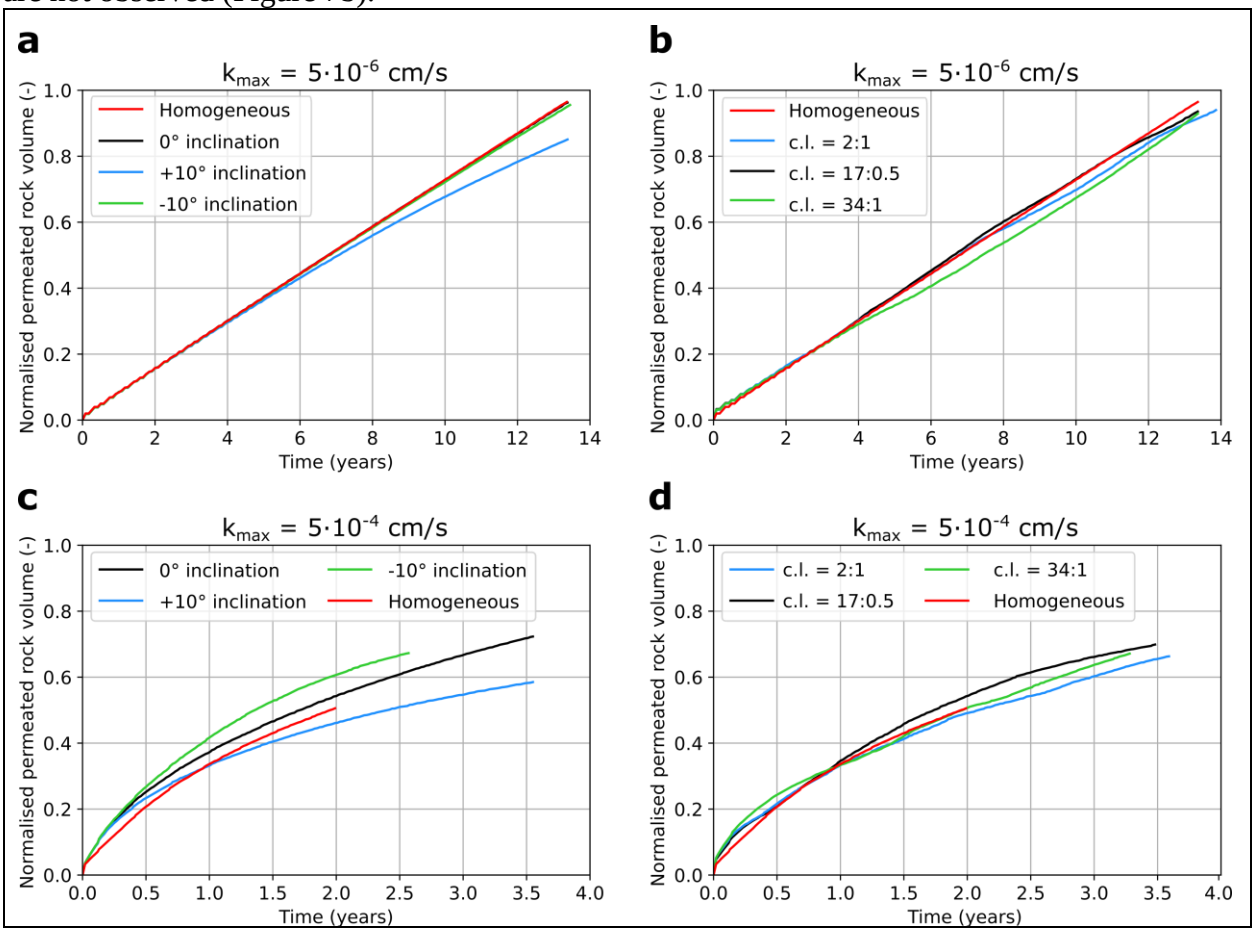

Figure 7. Ratio between permeated and total (soluble) rock volume over time for (a), (c) an intersecting halite layer and (b), (d) halite inclusions (c.l. = correlation length) compared to the homogeneous case.

In case of high dissolution rates (k_{max} = 5·10^{-4} cm/s), the differences between rock distributions increase (Figure 7c,d). Along a homogeneous potash seam, the leaching zone expands to the right model boundary in two years showing only a slight decrease in growth rate. However, only 50% of the rock become permeated, while the other half is not affected. In contrast, heterogeneous potash seams show permeation ratios of 59-72%, taking up to 3.6 years until the right model boundary is reached. Intersecting halite layer result in different evolutions depending on the inclination (Figure 7c). In case of a 0° inclination, the permeation speed is slightly faster than for the homogeneous case, but the stop criterion is only met when 72% of the rock are permeated. Therefore, it takes 3.6 years instead of the 2 years in the homogenous case. In case of a +10° inclination, the leaching zone growth is slower and only 60% of the rock are permeated within the same time period. An inclination of -10° (Figure 6c) causes the highest permeation speed with 2.6 years required to reach a 67% permeation or the right model boundary. Potash seams with halite inclusions show a very similar permeation speed compared to homogeneous ones (Figure 7d). However, since 66-70% of the (soluble) rock are permeated (instead of 50%), it takes the reaction front almost twice as long to arrive at the right model

boundary. Accordingly, heterogeneities slow down the leaching zone growth in horizontal direction by a factor of 1.25 to 1.8 in case of high dissolution rates.

In order to determine if the systems are transport- or reaction-dominated, and if the transport is dominated by advection or diffusion, the dimensionless parameters of Péclet (Pe) and Damköhler (Da) can be used, allowing for a classification into four different cases which show different temporal and spatial evolutions of the leaching zone (Steding et al., 2021). The Péclet number is determined from the flow velocity v, the diffusion coefficient D_f and the characteristic length l following equation (7). Pe has to be calculated individually for each cell, since v varies in space (and time). l is approximated with the current width of the leaching zone, which timely varies in vertical direction.

$$Pe = v \cdot l / D_f \tag{7}$$

To determine if the system is dominated by advection (Pe > 2) or diffusion (Pe < 2), the median of all permeated cells is determined. All homogeneous and heterogeneous scenarios show a median Péclet number which is clearly above two over the entire modelling period, i.e. all systems are advection-dominated. This means that diffusion is negligible as transport process within the leaching zone and that the Damköhler number, which is defined as the ratio between reaction rate and transport velocity, can be calculated from the flow velocity v according to equation (8). To calculate the reaction rate of each mineral, equation (1) is used considering the saturations of the inflowing solution. The studies of Field et al. (2019) indicate that at the same flow velocity, low saturations cause transport-dominated systems (Da > 1), while high saturations result in reaction-dominated systems (Da < 1). Since the solution at the left boundary is NaCl-saturated, the reaction rate for halite is zero. In case of sylvite and carnallite, *rate* corresponds to k_{max} since the inflowing solution is highly undersaturated with respect to both minerals. The transport velocity corresponds to the flow velocity calculated by TRANSE.

$$Da = \textit{reaction rate / transport velocity} = k_{max} / v \qquad \textit{(if Pe > 2)} \tag{8}$$

A Damköhler number for the system can be derived from k_{max} and the median of all flow velocities within the permeated area. The latter is divided into upper and lower halves in case of intersecting halite layers. Figure 8 shows that the median always ranges between 10^{-6} m/s and 10^{-8} m/s. This means that for $k_{max} = 5 \cdot 10^{-4}$ cm/s, Da is always above one, while for $k_{max} = 5 \cdot 10^{-6}$ cm/s, Da falls below one if the flow velocity is above $5 \cdot 10^{-8}$ m/s. In case of homogeneous potash seams, this holds true during the first 2 years of simulation (Figure 8a,b). After that, the decrease in flow velocity results in a Damköhler number slightly above one, eventually equalling 1.4. If the potash seam is intersected by a horizontal halite layer, it takes 3 years to reach Da = 1 since the average flow velocity is slightly higher at the beginning (Figure 8a). Later, its decrease is stronger, so that Da = 1.4 is eventually reached as well. Similar evolutions can be observed within the upper half of the potash seam if the intersecting halite layer is inclined. However, after 7-8 years, the flow velocity decrease becomes faster and Da becomes higher. On the other hand, flow velocities within the lower half are constantly lower for a +10° inclination and constantly higher for a -10° inclination. In the latter case, Da rises above one only after 13 years. In case of halite inclusions, it partly takes more than 2 years to reach Da = 1, e.g. for the 17:0.5 distribution, and the evolution of the average flow velocity is less regular resulting in several crossings of Da

= 1 over time, e.g. for the 34:1 distribution (Figure 8b). However, the overall evolution of flow velocities is relatively similar to the homogeneous case.

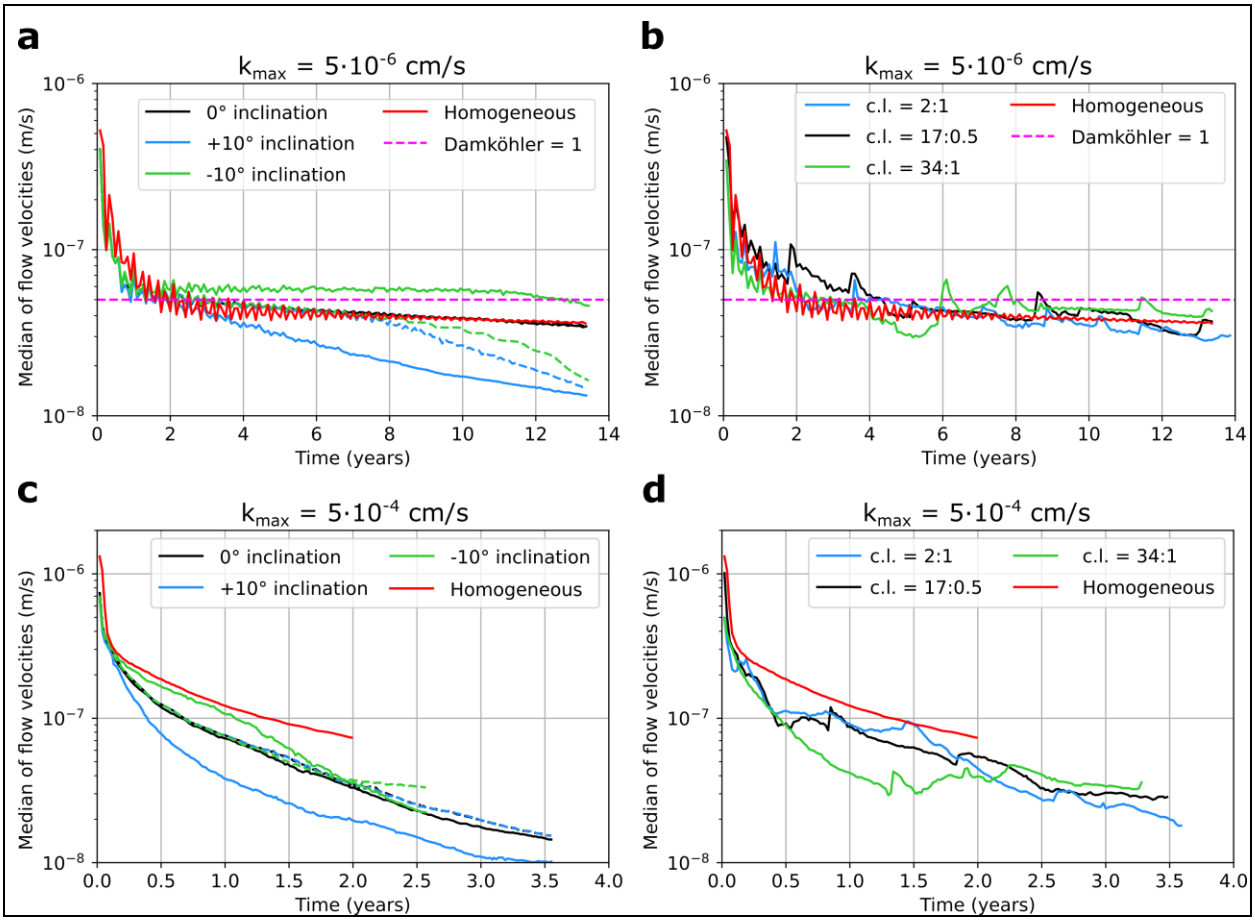

Figure 8. Median of flow velocities over time for (a), (c) an intersecting halite layer (solid line = below layer, dotted line = above layer) and (b), (d) halite inclusions (c.l. = correlation length) compared to the homogeneous case.

In contrast, k_{max} = 5·10^{-4} cm/s leads to larger deviations in flow velocity (Figure 8c,d). Thereby, heterogeneous potash seams generally show smaller flow velocities than homogeneous ones. In case of a horizontal, intersecting layer, both halves show the same decrease in flow velocity over time and after 2 years, the flow velocity amounts to approximately 50% of that in the homogeneous case (Figure 8c). The same evolution can be seen within the upper half of potash seams with intersecting layers at ±10° inclination. After 3.6 years, the flow velocities have decreased to 1.5·10^{-8} m/s, what represents only 20% of the final flow velocity in the homogeneous case. However, for a -10° inclination, the velocity decrease is reduced after 2 years and the right model boundary is reached after 2.6 years already. Within the lower half of the potash seam, the average flow velocity is smaller compared to the upper half if the inclination of the intersecting layer is +10°. In contrast, it is most of the time higher in case of -10° inclination. Thus, flow velocities within the lower half show an increased dependency on inclination. Heterogeneous potash seams with halite inclusions also show a clear trend towards flow velocity decrease over time (Figure 8d). However, phases of increase occur as well – especially for the

34:1 distribution – which cannot be observed for homogeneous potash seams or intersecting layers.

To evaluate the shift from reaction- (Da < 1) to transport-dominated (Da > 1) systems in case of k_{max} = 5·10^{-6} cm/s, the distribution of Mg^{2+} after different time periods is shown in Figure 9. The Mg^{2+} concentration is a useful indicator for fluid density and saturation: absence of Mg^{2+} usually represents a NaCl solution with a density of 1,200 kg/m^3, while a solution with >85 g/l Mg^{2+} (at 25 °C) has a density of >1,270 kg/m^3 and is fully saturated with respect to halite, sylvite and carnallite. In case of homogeneous potash seams (Figure 9), the solution is highly undersaturated with regard to sylvite and carnallite along the entire dissolution front during the first two years. Accordingly, both minerals are fully dissolved and only halite remains. In contrast to halitic areas, the rock is fully permeated and porosity is high (≈ 30%) within these zones (further referred to as halite zones). The dissolution front is planar during that time, while concentration and density gradients are comparatively low. However, the Mg^{2+} concentration at the bottom increases and after 2 years, when Da=1 is reached, the dissolution of sylvite and carnallite is significantly reduced at the lower end of the dissolution front. As a result, a sylvinitic zone, consisting of halite and sylvite (Figure 9d,e), is formed next to it and an inclination of the dissolution front occurs. Over time, its upper end moves upwards (Figure 9b,c) and the sylvinitic zone with lower porosity grows. Additionally, a small barrier is formed next to the lower end of the inflow due to the precipitation of halite (Figure 9d). Although the average flow velocity decreases (Figure 8a,b), the growth rate of the leaching zone remains constant over time (Figure 7a,b).

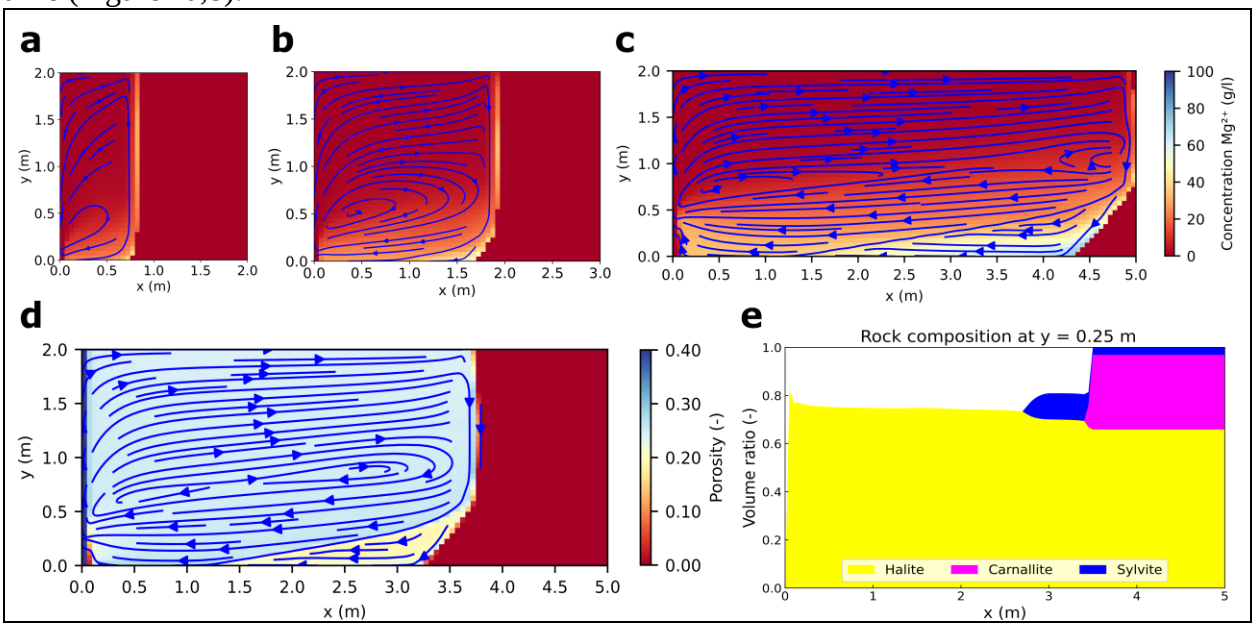

Figure 9. Convection cell of a system shifted from a reaction- to a transport-dominated one: Mg^{2+} concentration distribution after simulation times of (a) two years, (b) five years and (c) 13.4 years; (d) porosity distribution and (e) mineralogical composition after 10 years for a homogeneous potash seam and k_{max} = 5·10^{-6} cm/s.

In cases of halite inclusions, the leaching zone evolution is basically similar to the homogeneous case. However, the more often the dissolution front is disturbed by inclusions, the more irregular it becomes (Figure 10a-c). The same applies to the sylvinitic zone within the

lower area. Apart from that, sylvinitic zones now also occur above or behind inclusions and are often redissolved as soon as the flow regime changes and local Mg^{2+} concentrations decrease. A slower growth rate, which is usually associated with a sylvinitic zone next to the dissolution front, can now be observed within the upper area as well (Figure 10c). Generally, the convection cell is increasingly divided into smaller sub-cells, the broader inclusions are. However, with regard to the shape and penetration depth of the leaching zone, differences compared to the homogeneous case are negligible.

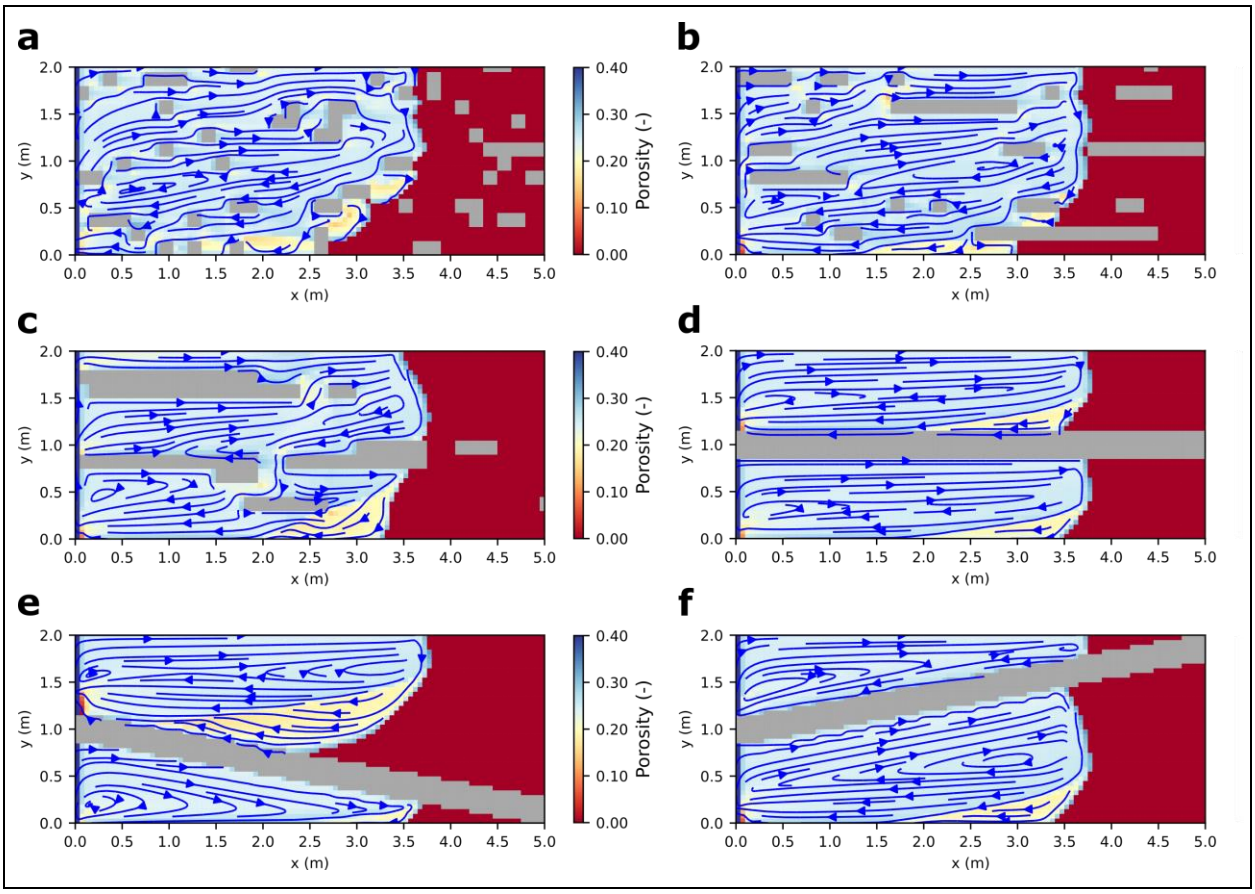

Figure 10. Porosity distribution after a simulation time of 10 years for heterogeneous potash seams with halitic inclusions for the distributions (a) 2:1, (b) 17:0.5, (c) 34:1 and intersecting layers with (d) 0°, (e) +10°, (f) -10° inclination and $k_{max} = 5 \cdot 10^{-6}$ cm/s.

In case of an intersecting, insoluble halite layer, the system is split up into two convection cells that evolve independently of each other. As shown in Figure 7a, the influence on the growth rate of the leaching zone is small if the dissolution rate is low ($k_{max} = 5 \cdot 10^{-6}$ cm/s). In case of a horizontal layer (Figure 10d), both convection cells show nearly the same evolution as that in the homogeneous case (Figure 9). Although the sylvinitic zone is formed slightly later – after about 3 years instead of 2 years – it quickly covers a larger part of the dissolution front: after 10 years, approximately 50% of it compared to 30% in the homogeneous case (Figure 9; 10d). However, the penetration depth at the upper end of the dissolution front is approximately the same. In contrast, the convection cells develop differently after some years if the intersecting layers are inclined (Figure 10e-f). Although the upper halves show similar flow velocities as in case of a horizontal layer during the first 7-8 years (Figure 8a), the sylvinitic zone is formed earlier and

grows faster if the height increases (Figure 10e), while it does not occur at all if the height decreases (Figure 10f). The same applies to the formation of the barrier next to the inflow. On the other hand, an increasing height within the lower half results in the same sylvinitic zone and barrier formation as in case of a horizontal layer (Figure 10d,f), although flow velocities are higher and it takes 13 years to reach Da=1 (Figure 8a). If the height within the lower half decreases, the sylvinitic zone starts forming after about 2.5 years but grows relatively slow. After 10.5 years, it completely covers the dissolution front (Figure 10e), although it is only 1 m wide and 0.2 m high. From that point in time, the growth rate of the lower half is reduced, while flow velocities already show a significant decrease after 3 years (Figure 8a). In all other cases, the maximum penetration depth is the same within the upper and lower layer and the right model boundary is reached after 13.4 years.

For $k_{max} = 5 \cdot 10^{-4}$ cm/s, the Damköhler number is clearly above one during the entire simulation time and a funnel-shaped leaching zone is formed, showing preferential dissolution within the upper half of the potash seam (Figure 11). Its width decreases nearly linearly from the top to the bottom. The lower part of the potash seam is not dissolved, resulting in an increased flattening of the dissolution front over time. As indicated in Figure 7c-d, the expansion becomes slower over time: while the leaching zone penetrates 3 m deep into the seam in the first year, it proceeds only two more metres into the seam within the second year. The precipitation of halite next to the left model boundary leads to the formation of a flow barrier within the lower half of the potash seam. Close to the entire dissolution front, a sylvinitic zone is formed (Figure 11a, yellow). Its maximum width in horizontal direction is reached at the height of the barrier top. Basically, two different solution compositions exist within the leaching zone. The first one contains almost no Mg^{2+} and can be found within the halite zone (Figure 11a, blue), while the second one shows Mg^{2+} concentrations of >70 g/l and is present within the sylvinitic zone (Figure 11a, yellow). The border reaches from the upper end of the dissolution front to the top of the barrier and represents an area with large concentration gradients. Thus, there is a large density gradient at the border as well, representing the driving force of the free convection. Figure 11a shows that above this border, fluid flow proceeds mainly from left to right, while below it the (highly saturated) solution is moving from the dissolution front back towards the left boundary. The resulting flow velocities are higher at the beginning compared to $k_{max} = 5 \cdot 10^{-6}$ cm/s, but show a stronger decrease over time (Figure 8).

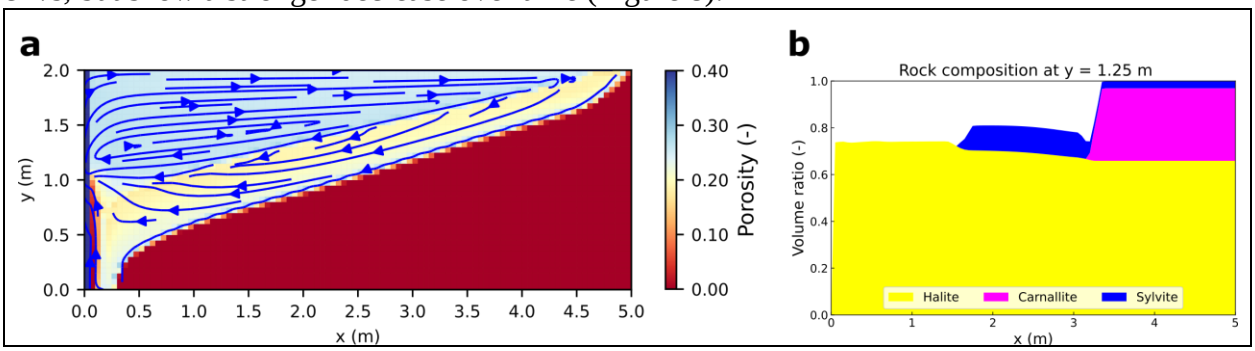

Figure 11. Convection cell of a fully transport-dominated system: (a) Porosity distribution and (b) mineralogical composition after a simulation time of 2 years for a homogeneous potash seam and $k_{max} = 5 \cdot 10^{-4}$ cm/s

In case of $k_{max} = 5 \cdot 10^{-4}$ cm/s, halite inclusions lead to smaller, less regular flow velocities in space and time (Figure 8d). In case of small and medium-sized inclusions, the flow field still

shows one main convection cell with undersaturated inflowing solution, mainly present within the upper-left area of the leaching zone, and highly saturated outflowing solution along the dissolution front and within the lower area (Figure 12a,b). Accordingly, the shape of sylvinitic zone and barrier remains basically similar to the homogeneous case. However, zones containing only halite now also occur within the lower half of the leaching zone behind the barrier. In return, wide sylvinitic zones can occur in the upper half especially above inclusions (Figure 12b). Neither the inclination of the dissolution front nor of the border between the halite and sylvinitic zone is linear any more and the lower end of the dissolution front is about 1 m away from the inflow compared to 0.25 m in the homogeneous case (Figure 11a; 12a,b). In case of broader inclusions, the flow field shows three smaller convection cells after 10 years with each having its own barrier at the left (Figure 12c). The same applies to the sylvinitic zone. The dissolution front is subdivided into 3-4 sections with different penetration depths. Thereby, the upper one shows lower dissolution rates than the one below, leading to a recess at 1.6 m height. However, this phenomenon quickly disappears as soon as the upper half of the dissolution front is not subdivided any more and the flow regime changes accordingly. Between large inclusions, the flow is not disturbed and the dissolution front as well as the borders between halite and sylvinitic zones are nearly as regular as in the homogeneous case (Figure 11a). However, the overall inclination of the dissolution front is much steeper. As a result, the same permeation speed leads to smaller penetration depths within the upper part of the potash seam after 2 years, but higher

permeation ratios at the end for all cases of halite inclusions (Figure 7d). Here, the right model boundary is reached after 3.3 years (34:1) to 3.6 years (2:1).

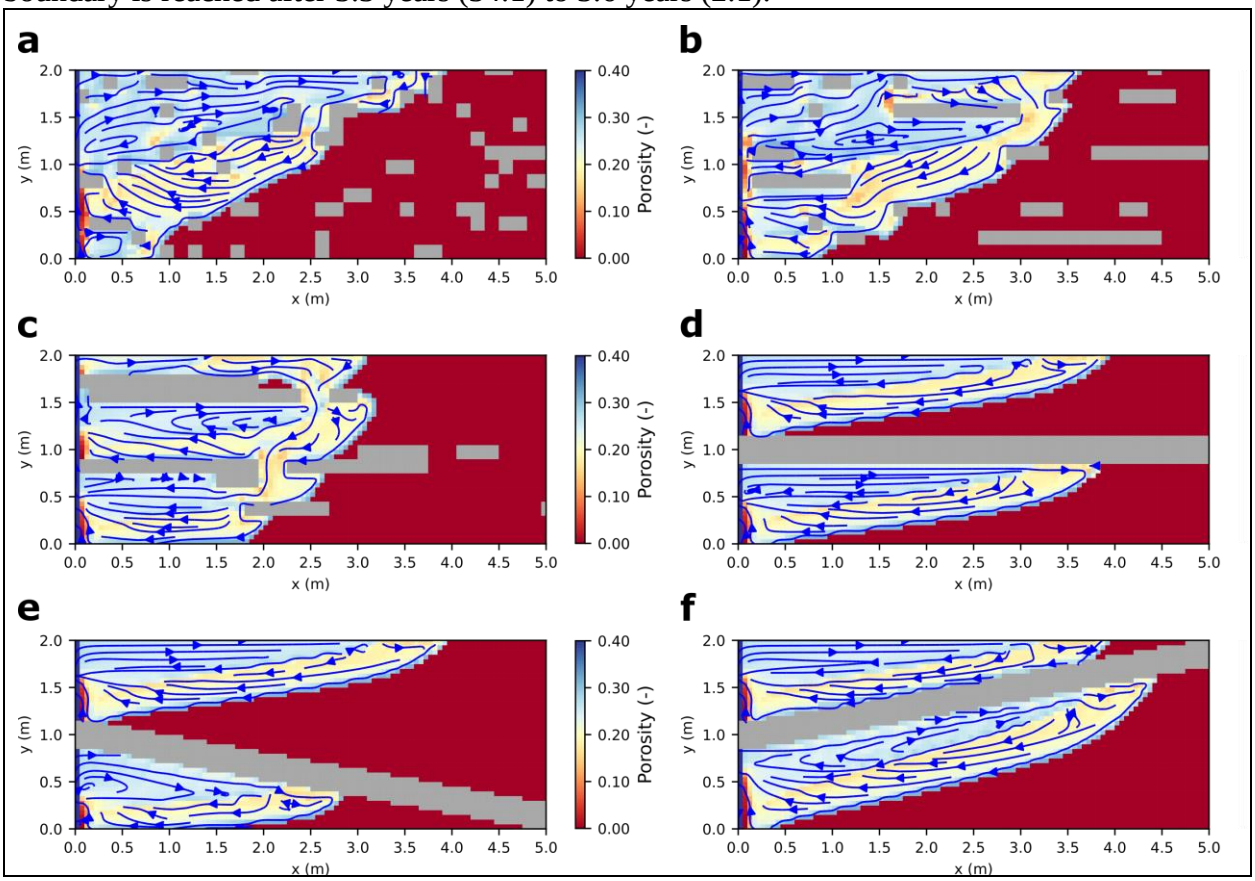

Figure 12. Porosity distribution after a simulation time of 2 years for heterogeneous potash seams with halitic inclusions for distributions of (a) 2:1, (b) 17:0.5, (c) 34:1 and intersecting layers with (d) 0°, (e) +10°, (f) -10° inclination and $k_{max} = 5 \cdot 10^{-4}$ cm/s.

The leaching zones above intersecting layers show nearly similar evolutions in penetration depth regardless of the inclination (Figure 12d-f). If the height is constant or increases, shape and flow velocities evolve similarly as well (Figure 12d,e; 8d), while in case of decreasing height, the dissolution front follows the intersecting layer (Figure 12f) and the penetration speed slightly decreases as the height falls below 0.25 m. Compared to the homogeneous case, the width of the leaching zone shows a lower decrease within the upper half and a higher one within the lower half, resulting in higher permeation ratios (Figure 7c). Only if the height increases, a large area of undissolved potash salt is maintained between the intersecting layer and the upper leaching zone, leading to an overall permeation ratio of 59% (compared to >70% for 0° and -10° inclination) at the end of the simulation time (Figure 7c; 12e). After 2 years, the barrier covers about half of the upper in- and outflow region and the right model boundary is reached after 3.5 years. However, in case of a -10° inclination, the lower leaching zone grows faster than the upper one (Figure 12f). Thus, the right model boundary is already reached after 2.6 years. In contrast, the +10° inclination results in smaller growth rates within the lower half (Figure 12e). Generally, layers with increasing height grow faster, while layers with decreasing height show higher permeation ratios (Figure 12e,f). Compared to the

homogeneous case, sylvinitic zones (yellow) are slightly broader at the upper end of the dissolution front in all cases of intersecting layers.

4 Discussion

The results show that the influence of insoluble inclusions and intersecting layers strongly depends on the dissolution rate of the soluble minerals. In case of low dissolution rates ($k_{max} = 5 \cdot 10^{-6}$ cm/s), the evolution of the leaching zone is only slightly affected (Figure 7a,b; 10), although local and average flow velocities are significantly changed (Figure 8a,b). In contrast, heterogeneities lead to a reduction in penetration depth (Figure 12) and higher permeation ratios (Figure 7c,d) if dissolution rates are high ($k_{max} = 5 \cdot 10^{-4}$ cm/s). These differences can be explained by a distinction between reaction-dominated and transport-dominated systems. A fully reaction-dominated system (Da << 1) is given if the effective dissolution rates of sylvite and carnallite according to equation (1) correspond to the maximum dissolution rate, i.e. if their saturation only shows a very slight increase along the dissolution front. In this case, the dissolution front is planar and neither local nor overall changes in flow velocity affect the growth rate of the leaching zone: it is entirely controlled by the reaction speed. This case is given for $k_{max} = 5 \cdot 10^{-6}$ cm/s at the start of the simulation. However, after some years, the saturations along the dissolution front become high enough to significantly reduce the dissolution rate of sylvite and carnallite, making the system only partly reaction-dominated (Da ≈ 1). The reason for that can be a decrease in flow velocity or an increase in the length of the dissolution front. As a result, the dissolution front becomes inclined and a sylvinitic zone as well as a barrier are formed (Figure 9). If the entire dissolution front is inclined and covered by a sylvinitic zone, the system is fully transport-dominated (Da >> 1) as given for $k_{max} = 5 \cdot 10^{-4}$ cm/s. These systems are much more sensitive to changes in flow velocity. Therefore, they are much more affected by heterogeneities influencing both, the local distribution and the average flow velocity (Figure 8; 10; 12).

The Damköhler number is a useful indicator to determine if a system is dominated by reaction or transport (Weisbrod et al., 2012; Oltéan et al., 2013; Steding et al., 2021). Generally, the simulation results show that an overall Da calculated from the average flow velocity and the saturation-dependent dissolution rate of the inflowing solution corresponds to the observed leaching zone shapes. In case of $k_{max} = 5 \cdot 10^{-4}$ cm/s, Da >> 1 is given and a funnel-shape can be observed including a barrier at the left and a sylvinitic zone along the entire dissolution front (Figure 11). These are typical indicators for a transport-dominated system (Steding et al., 2021). In case of $k_{max} = 5 \cdot 10^{-6}$ cm/s, the dissolution front is planar in the beginning when Da < 1, while it becomes inclined as Da rises above one with a sylvinitic zone and barrier rising from the bottom (Figure 8a,b; 9a-c). However, insoluble inclusions make it more difficult to identify this point in time, because the average flow velocity evolves less regularly (Figure 8b) and strong local deviations occur, resulting in small sylvinitic zones near the inclusions and a more irregular dissolution front (Figure 10a-c). In case of intersecting layers, Da has to be determined for each sub-system or convection cell, and if the layer is inclined, the time period in which Da rises above one does no longer correlate with the formation of sylvinitic zones and barriers (Figure 8a; 10d-f). From our point of view, the reason for this is a change in the length of the dissolution front: if it increases, higher saturations can be reached at the bottom without a change in flow velocity and vice versa. All in all, the larger the heterogeneities are, the less appropriate an overall Damköhler number is to determine if the system is dominated by reactions or transport. Additionally, it has to be noted that complex systems containing several minerals can be reaction- and transport-dominated at once: if the maximum dissolution rate k_{max} or the saturations

of the inflowing solution vary a lot for different minerals, some of them will show Da > 1, while others show Da < 1. Accordingly, the Damköhler number has to be calculated individually for each mineral and an internal contact area between equilibrated and non-equilibrated minerals has to be defined (Figure 4) to reproduce the formation of several dissolution fronts as those observed by Ahoulou et al. (2020). In this case, heterogeneities are expected to mainly influence the dissolution pattern of minerals with Da > 1.

Heterogeneities also affect the hazard potential of leaching zones by influencing the growth rate, shape and permeation ratio. In this context, higher growth rates are associated with faster expansion of the leaching zone and an increasing risk of mine flooding or integrity loss of a cavern. Higher permeation ratios or porosities also increase the hazard potential as they result in a lower mechanical stability as well as larger solution amounts stored per metre leaching zone. The results show that for Da >> 1, insoluble inclusions mainly affect the shape: at the top, the dissolution front is progressing relatively slow, whereas at the bottom dissolution rates are higher compared to the homogeneous case (Figure 11; 12a-c). As a result, the permeation speed is basically the same (Figure 7d), but the dissolution front is steeper and it takes 1.65-1.8 times longer until the right model boundary is reached. It is important to note that the distribution of insoluble inclusions does not have a significant influence if their volume ratio is identical. Although broader inclusions increasingly split up the convection cell into smaller ones and lead to a more irregular average flow velocity, the overall evolution is always quite similar (Figure 7d; 8d; 12a-c). Thereby, the leaching zone growth in horizontal direction is slower compared to the homogeneous case, but the permeation ratio is higher at the end of the simulation, what can become more critical with regard to mechanical stability. In case of one continuous insoluble layer, the leaching zone consists of two independent convection cells, showing the same regular dissolution front, sylvinitic zone and barrier as in the homogeneous case. However, flow velocities and permeation speed are more similar to those of insoluble inclusions (Figure 7c; 8c; 12d). Inclined, intersecting layers particularly influence the flow velocity within the lower half (Figure 8c). Thereby, negative inclinations increase the flow velocity resulting in faster leaching zone growth compared to the upper half (Figure 12f) and vice versa. The evolution of the upper half is basically not influenced (Figure 12e,f). However, the amount of undissolved potash rock is larger with increasing height, resulting in relatively small permeation ratios (Figure 7c). In summary, an intersecting layer with negative inclination is the most critical distribution of insoluble inclusions, leading to higher permeation ratios and only slightly smaller growth rates in horizontal direction compared to the homogeneous case.

Field observations indicate that the formation of caverns and leaching zones in salt rock is usually dominated by transport. According to Koch and Vogel (1980), the upper half of a potash seam is often preferentially dissolved and natural leaching zones within carnallitic rock are mostly divided into a halite zone near the inflow region and a sylvinitic zone close to the dissolution front. These observations agree with the results for a transport-dominated system ($k_{max} = 5 \cdot 10^{-4}$ cm/s) of homogeneous rock composition (Figures 11). In case of intersecting layers from pure halite, Koch and Vogel (1980) assume a split into several dissolution fronts with different penetration depths. A similar phenomenon has been observed in solution mining: if several insoluble layers cross the salt body, the resulting cavern shape resembles an inverted Christmas tree (Thoms & Gehle, 1999). The same shape is described by Fokker (1995) for technical caverns crossing different (potash) salt layers. Furthermore, Fokker (1995) implies that inclined layers cause an asymmetric shape, whereby the growth rate is faster in the direction of

upward-directed inclination. These descriptions all correspond to the simulation results for a transport-dominated system with intersecting halite layers (Figures 12d-f). However, time frames for the evolution of natural leaching zones are not available. Regarding insoluble inclusions, laboratory experiments conducted by Gechter et al. (2008) and Field et al. (2019) confirm that the cavern shape becomes increasingly distorted and notches occur at the dissolution front if insoluble lenses impede regular fluid flow (Figures 12a-c). Also consistent is the finding that inclusions do not reduce the amount of dissolved/permeated rock per time but only its distribution (Figures 7d) (Gechter et al., 2008). Reaction-dominated systems with (nearly) planar dissolution fronts only occur if the inflowing solution is already highly saturated with respect to the present salt minerals (Field et al., 2019). In this case, significantly slower growth rates as well as an increased influence of rock fabric were observed. The first finding agrees with our simulation results (Figures 7), while the second one could not be reproduced (Figures 10a-c). All in all, there is a good correlation between literature data and model results regarding the influence of heterogeneities. However, the temporal scaling is still uncertain and more data are required for a comprehensive quantitative model validation.

Finally, the results reveal how saturation-dependent dissolution rates affect barrier formation and leaching zone shape. In case of fully reaction-dominated systems (Da << 1), there is no difference compared to constant dissolution rates because k_{max} is always reached. In contrast, transport-dominated systems show a more linear decrease in width from the top to the bottom, since the effective dissolution rate decreases along the dissolution front. Therefore, a longer distance is required until the solution is fully saturated and the transition from dissolved to undissolved sections of the potash seam is less sharp compared to constant dissolution rates (Steding et al., 2021). Additionally, the barrier next to the inflow is smaller, resulting in a less decreasing flow velocity and growth rate over time. Thus, saturation-dependent dissolution rates lead to a wider extension and therefore a higher hazard potential of the leaching zone in the long term. Furthermore, they intensify the coupling between chemical reactions and transport. Next to the dissolution front, where strong concentrations gradients occur, changes in advection, diffusion or dispersion immediately affect the saturations, and therefore the effective dissolution rates. In return, the dissolved mineral amounts affect transport parameters such as brine density, viscosity and diffusion coefficients. An even stronger coupling would be achieved if k_{max} is treated as a function of flow velocities. Several studies indicate that for fast dissolving minerals, such as most potash salts, the dissolution rate is controlled by the transport across a so-called diffusive boundary layer that is formed at the mineral-fluid interface (Alkattan et al., 1997; De Baere et al., 2016; Dutka et al., 2020). Thereby, higher fluid flow velocities induce a decrease in thickness of the boundary layer, and therefore higher dissolution rates of the minerals. As a result, k_{max} varies locally and heterogeneities may have a stronger effect. However, the approach uses input parameters, such as the reaction rate constant, which are currently not known for many potash minerals. Furthermore, knowledge about the flow field at pore scale and the bulk concentrations outside the boundary layer are required (Molins et al., 2012). Both are hard to determine by continuum-scale models which cannot exactly reproduce the concentration distribution at the dissolution front. By using average saturations to calculate the dissolution rates, an artificial mixing is always generated, influencing the leaching zone shape or the fluid flow path until full saturation is reached. Accordingly, a calibration of the model based on experimental data is crucial. All in all, the simulation results show that the saturation-dependency of dissolution rates has a significant influence on the leaching zone evolution in case

699 of partly or fully transport-dominated systems (Da ≥ 1), and therefore needs to be considered
700 when investigating further scenarios.

701 **5 Conclusions and outlook**

702 The reactive transport model presented here takes into account the local saturation state
703 of each mineral for the calculation of its dissolution rate. As a result, highly undersaturated
704 minerals are dissolved relatively fast, while others remain undissolved. In case of the carnallite-
705 bearing potash seam used for our scenario analysis, areas from pure halite are insoluble because
706 the inflowing solution is constantly NaCl-saturated. The results show that insoluble inclusions
707 and intersecting layers mainly influence the evolution of advection- and transport-dominated
708 systems (Pe > 2 and Da > 1). Thereby, the amount of potash salt permeated over time is similar
709 to the homogeneous case, whereas the shape of the leaching zone is different. Although the
710 upper half of the potash seam is still preferentially dissolved, the dissolution front becomes
711 steeper in case of insoluble inclusions. In case of intersecting layers, two independent leaching
712 zones evolve. All cases have in common that the upper end of the dissolution front(s) moves
713 forward 1.8 times slower and, in return, the permeation ratio of the potash seam increases from
714 50% to 59-72% at the end of the simulation time. Interestingly, the distribution of the insoluble
715 areas is of minor importance: only if these appear as an intersecting layer with negative
716 inclination, the growth rate is 1.25 times lower instead of 1.8. Generally, inclined layers result in
717 an asymmetric expansion of the leaching zone with the upward-directed inclination showing
718 faster growth rates. In case of advection- and reaction-dominated systems (Pe > 2 and Da < 1),
719 the influence of heterogeneities on the leaching zone evolution is negligible. Although the
720 dissolution front becomes less regular, the growth rate, shape and porosity of the leaching zone
721 remain basically unaffected. Literature data indicate that most systems in nature are transport-
722 dominated.

723 With regard to risk assessment, insoluble areas within potash seams can usually be seen
724 as beneficial. At best, they slow down leaching zone growth, while at worst they do not. In order
725 to asses their influence, the Damköhler number is a useful indicator that can be determined from
726 the average flow velocity and the effective dissolution rate(s) of the inflowing solution.
727 However, Da has to be calculated individually for each mineral and, in case of intersecting
728 layers, also for each separate leaching zone. Heterogeneities influence the local and average flow
729 velocities and can shift the transition time from a reaction- to a transport-dominated system.
730 Especially inclined intersecting layers reduce the validity of the Da indicator. However, the
731 occurrence of funnel-shapes, barriers and sylvinitic zones (in case of carnallitic potash salt), can
732 be seen as a clear evidence for transport-dominated systems (Da > 1). In contrast, planar
733 dissolution fronts and an effluent solution that is not fully saturated with regard to the present
734 minerals indicate a reaction-dominated system (Da < 1). The first kind of systems evolves
735 generally faster in the beginning, but the growth rate is reduced by barrier formation and
736 heterogeneities (if present). However, it has to be noted that with regard to the solution amount
737 and mechanical stability, heterogeneities may increase the hazard potential due to the higher
738 permeation ratios of 59-72%. Reaction-dominated systems show a slow but steady growth that is
739 not reduced by heterogeneities. The potash seam becomes fully permeated and all minerals
740 undersaturated with regard to the inflowing solution are dissolved. Thus, the collapse of
741 insoluble layers and/or large inclusions as described by Anderson and Kirkland (1980) or Warren

(2017) has to be considered if the mechanical stability of the remaining rock matrix is insufficient.

The extension of the reactive transport model by variable saturation-dependent dissolution rates has improved its accuracy with regard to leaching zone shape, growth rate and barrier formation. It is shown that constant dissolution rates overestimate the barrier formation, and therefore underestimate the hazard potential in the long-term. In the next step, it is planned to not only distinguish between insoluble and highly soluble minerals but to also include slower dissolving minerals such as anhydrite ($CaSO_4$) or kieserite ($MgSO_4 \cdot H2O$) into the model by using individual maximum dissolution rates. In doing so, the effects of mineral heterogeneity (Liu et al., 2017) can be investigated in further detail. However, for many secondary minerals occurring in these complex quinary or hexary systems (Steding et al., 2020), k_{max} is not known. Furthermore, a dependency on the local flow velocity is expected to intensify the coupling between chemical reactions and transport. Therefore, laboratory and field measurement data are required to calibrate k_{max} and, on this basis, to model the evolution of leaching zones within potash seams of any composition in space and time.

Acknowledgments

The authors like to thank the German Federal Ministry of Education and Research for the financial support of the project. Furthermore, we thank Axel Zirkler and Dr. Thomas Radtke from K+S for many informative discussions and useful pieces of advice regarding the model conceptualization.

Availability Statements

Datasets have not been used for this publication.

The software GSTools and PHREEQC are available in these in-text data citation references: Müller & Schüler (2021), Parkhurst & Appelo (2013)

The software TRANSE is described in Kempka (2020) with the code being currently in publication process.

The coupling of PHREEQC and TRANSE was done in Python 3 which is available in this in-text data citation reference: Van Rossum & Drake (2009).

The model output data and the Jupyter notebook to execute the analysis in the paper will be published via GFZ Data Services (https://dataservices.gfz-potsdam.de/portal/about.html) and are currently (for an exemplary scenario) available at Nextcloud via https://nextcloud.gfz-potsdam.de/s/QcQmgf5QAqzwoTQ.

References

Ahoulou, A.W.A., Tinet, A.J., Oltéan, C. & Golfier, F. (2020), Experimental Insights Into the Interplay Between Buoyancy, Convection, and Dissolution Reaction. *Journal of Geophysical Research: Solid Earth*, *125*(11), 1–18. doi:10.1029/2020JB020854

Alkattan, M., Oelkers, E., Dandurand, J. & Schott, J. (1997), Experimental studies of halite dissolution kinetics, 1 The effect of saturation state and the presence of trace metals. *Chemical Geology*, *137*(3–4), 201–219. doi:10.1016/S0009-2541(96)00164-7

Altmaier, M., Brendler, V., Bube, C., Neck, V., Marquardt, C., Moog, H.C., Richter, A., Scharge, T., et al. (2011), *THEREDA - Thermodynamische Referenz-Datenbasis* (Rep. 265). Braunschweig, Germany: Gesellschaft für Anlagen- und Reaktorsicherheit (GRS). Retrieved from https://www.thereda.de/en/

Anderson, R.Y. & Kirkland, D.W. (1980), Dissolution of salt deposits by brine density flow. *Geology, 8*(2), 66–69. doi:10.1130/0091-7613(1980)8<66:DOSDBB>2.0.CO;2

Boys, C. (1993), A Geological Approach to Potash Mining Problems in Saskatchewan, Canada. *Exploration and Mining Geology, 2*(2), 129–138.

De Baere, B., Molins, S., Mayer, K.U. & François, R. (2016), Determination of mineral dissolution regimes using flow-through time-resolved analysis (FT-TRA) and numerical simulation. *Chemical Geology, 430*(2016), 1–12. doi:10.1016/j.chemgeo.2016.03.014

Dijk, P.E. & Berkowitz, B. (2000), Buoyancy-driven dissolution enhancement in rock fractures. *Geology, 28*(11), 1051–1054. doi:10.1130/0091-7613(2000)28<1051:BDEIRF>2.0.CO;2

Dreybrodt, W. & Buhmann, D. (1991), A mass transfer model for dissolution and precipitation of calcite from solutions in turbulent motion. *Chemical Geology, 90*(1–2), 107–122. doi:10.1016/0009-2541(91)90037-R

Durie, R.W. & Jessen, F.W. (1964), Mechanism of the Dissolution of Salt in the Formation of Underground Salt Cavities. *Society of Petroleum Engineers Journal, 4*(02), 183–190. doi:10.2118/678-pa

Dutka, F., Starchenko, V., Osselin, F., Magni, S., Szymczak, P. & Ladd, A. J.C. (2020), Time-dependent shapes of a dissolving mineral grain: Comparisons of simulations with microfluidic experiments. *Chemical Geology, 540*(2019), 119459. doi:10.1016/j.chemgeo.2019.119459

Field, L.P., Milodowski, A.E., Evans, D., Palumbo-Roe, B., Hall, M.R., Marriott, A.L., Barlow, T. & Devez, A. (2019), Determining constraints imposed by salt fabrics on the morphology of solution-mined energy storage cavities, through dissolution experiments using brine and seawater in halite. *Quarterly Journal of Engineering Geology and Hydrogeology, 52*(2), 240–254. doi:10.1144/qjegh2018-072

Fokker, P.A. (1995) *The behaviour of salt and salt caverns* (Doctoral dissertation). Retrieved from: http://repository.tudelft.nl/view/ir/uuid:6847f8e4-3b09-4787-be02-bcce9f0eed06/.

Gechter, D., Huggenberger, P., Ackerer, P. & Niklaus Waber, H. (2008), Genesis and shape of natural solution cavities within salt deposits. *Water Resources Research, 44*(11), 1–18. doi:10.1029/2007WR006753

Höntzsch, S. & Zeibig, S. (2014). *Geogenic caverns in rock salt formations - a key to the understanding of genetic processes and the awareness of hazard potential* Poster presented at GeoFrankfurt 2014, Frankfurt a.M., Germany.

Hoppe, H. & Winkler, F. (1974), Beitrag zur Lösekinetik von Mineralien der Kaliindustrie. *Wissenschaftliche Zeitschrift Techn. Hochsch. Chem. Leuna-Merseburg, 16(1)*, 23–28.

Jinlong, L., Wenjie, X., Jiangjing, Z., Wei, L., Xilin, S. & Chunhe, Y. (2020), Modeling the mining of energy storage salt caverns using a structural dynamic mesh. *Energy, 193*, 116730. doi:10.1016/j.energy.2019.116730

Keime, M., Charnavel, Y., Lampe, G. & Theylich, H. (2012). *Obstruction in a salt cavern : Solution is dissolution* Paper presented at World Gas Conference 2012, Kuala Lumpur, Malaysia.

Kempka, T. (2020), Verification of a Python-based TRANsport Simulation Environment for density-driven fluid flow and coupled transport of heat and chemical species. *Advances in Geosciences, 54*, 67-77. doi:10.5194/adgeo-54-67-2020

Koch, K. & Vogel, J. (1980). Zu den Beziehungen von Tektonik, Sylvinitbildung und Basaltintrusionen im Werra-Kaligebiet (DDR). *Freiberger Forschungshefte*.(C 347). Leipzig: VEB Deutscher Verlag für Grundstoffindustrie.

Li, J., Shi, X., Yang, C., Li, Y., Wang, T. & Ma, H. (2018), Mathematical model of salt cavern leaching for gas storage in high-insoluble salt formations. *Scientific Reports, 8*(1), 372. doi:10.1038/s41598-017-18546-w

Liu, M., Shabaninejad, M. & Mostaghimi, P. (2017), Impact of mineralogical heterogeneity on reactive transport modelling. *Computers and Geosciences, 104*, 12–19. doi:10.1016/j.cageo.2017.03.020

Mengel, K., Röhlig, K.J. & Geckeis, H. (2012), Endlagerung radioaktiver Abfälle. *Chemie in Unserer Zeit, 46*(4), 208–217. doi:10.1002/ciuz.201200582

Molins, S., Trebotich, D., Steefel, C.I. & Shen, C. (2012), An investigation of the effect of pore scale flow on average geochemical reaction rates using direct numerical simulation. *Water Resources Research, 48*(3), 1–11. doi:10.1029/2011WR011404

Müller, S. & Schüler, L. GeoStat-Framework/GSTools. *Zenodo*. doi:10.5281/zenodo.1313628

Oltéan, C., Golfier, F. & Buès, M.A. (2013), Numerical and experimental investigation of buoyancy-driven dissolution in vertical fracture. *Journal of Geophysical Research: Solid Earth, 118*(5), 2038–2048. doi:10.1002/jgrb.50188

Palandri, J.L. & Kharaka, Y.K. (2004), *A compilation of rate parameters of water-mineral interaction kinetics for application to geochemical modeling* (Rep. 2004/1068). Menlo Park, CA: U.S. Geological Survey (USGS). Retrieved from: http://www.dtic.mil/cgi-bin/GetTRDoc?Location=U2&doc=GetTRDoc.pdf&AD=ADA440035

Parkhurst, D.L. & Appelo, C.A.J. (2013). Description of Input and Examples for PHREEQC Version 3 - a Computer Program for Speciation, Batch-reaction, One-dimensional Transport, and Inverse Geochemical Calculations. In *Techniques and Methods* (book 6, chapter A43, 497 p.). Denver, CO: U.S. Geological Survey (USGS). doi:10.3133/tm6A43

Prugger, F.F. & Prugger, A.F. (1991), Water problems in Saskatchewan potash mining - what can be learned from them?. *Underground Mining, 84*(945), 58–66.

Raines, M.A. & Dewers, T.A. (1997), Mixed transport/reaction control of gypsum dissolution kinetics in aqueous solutions and initiation of gypsum karst. *Chemical Geology, 140*(1–2), 29–48. doi:10.1016/S0009-2541(97)00018-1

Röhr, H.U. (1981), Lösungsgeschwindigkeiten von Salzmineralen beim Ausspülen von Hohlräumen im Salz. *Kali und Steinsalz, 8*(4), 103–111.

Steding, S., Kempka, T., Zirkler, A. & Kühn, M. (2021), Spatial and temporal evolution of leaching zones within potash seams reproduced by reactive transport simulations. *Water, 13*(2). doi:10.3390/w13020168

Steding, S., Zirkler, A. & Kühn, M. (2020), Geochemical reaction models quantify the composition of transition zones between brine occurrence and unaffected salt rock. *Chemical Geology, 532*, 119349. doi:10.1016/j.chemgeo.2019.119349

Thoms, R.L. & Gehle, R.M. (1999), Non-halites and fluids in salt formations, and effects on cavern storage operations. *Geotechnical Special Publication, 90*, 780–796.

Warren, J.K. (2017), Salt usually seals, but sometimes leaks: Implications for mine and cavern stabilities in the short and long term. *Earth-Science Reviews, 165*, 302–341. doi:10.1016/j.earscirev.2016.11.008

Van Rossum, G., & Drake, F.L. (2009), *Python 3 Reference Manual* (Version 3.7.9). Scotts Valley, CA: CreateSpace. Retrieved from: https://www.python.org/downloads/

Wei, W., Varavei, A., Sanaei, A. & Sepehrnoori, K. (2019), Geochemical Modeling of Wormhole Propagation in Carbonate Acidizing Considering Mineralogy Heterogeneity. *SPE Journal, 24*(05), 2163–2181. doi:10.2118/195593-pa

Weisbrod, N., Alon-Mordish, C., Konen, E. & Yechieli, Y. (2012), Dynamic dissolution of halite rock during flow of diluted saline solutions. *Geophysical Research Letters, 39*(9), L09404. doi:10.1029/2012GL051306

Xie, M., Kolditz, O. & Moog, H.C. (2011), A geochemical transport model for thermo-hydro-chemical (THC) coupled processes with saline water. *Water Resources Research, 47*(2), W02545. doi:10.1029/2010WR009270

Yang, X., Liu, X., Zang, W., Lin, Z. & Wang, Q. (2017), A Study of Analytical Solution for the Special Dissolution Rate Model of Rock Salt. *Advances in Materials Science and Engineering, 2017*, 1–8. doi:10.1155/2017/4967913

Yuan-Hui, L. & Gregory, S. (1974), Diffusion of ions in sea water and in deep-sea sediments. *Geochimica et Cosmochimica Acta, 38*(5), 703–714. doi:10.1016/0016-7037(74)90145-8